# A co-opted ISG15-USP18 binding mechanism normally reserved for deISGylation controls type I IFN signalling

Andri Vasou[1], Katie Nightingale[2], Vladimíra Cetkovská [1], Connor G.G. Bamford[3‡], Jelena Andrejeva[1], Richard E. Randall[1], John McLauchlan[3], Michael P. Weekes[2], David J Hughes[1]*

[1]Biomedical Sciences Research Complex, School of Biology, University of St Andrews, St Andrews, United Kingdom. [2]Cambridge Institute for Medical Research, Hills Road, Cambridge, United Kingdom [3]MRC-University of Glasgow Centre for Virus Research, Glasgow, United Kingdom.

‡ Present addresses: Wellcome-Wolfson Institute for Experimental Medicine, Queen's University, Belfast UK.

* Corresponding author: djh25@st-andrews.ac.uk; Tel: +44 1334 467197

**Abstract**

Type I interferon (IFN) signalling induces the expression of several hundred IFN-stimulated genes that provide an unfavourable environment for viral replication. To prevent an overexuberant response and autoinflammatory disease, IFN signalling requires tight control. One critical regulator is the ubiquitin-like protein ISG15, evidenced by autoinflammatory disease in patients with inherited ISG15 deficiencies. Current models suggest that ISG15 stabilises USP18, a well-established negative regulator of IFN signalling. USP18 also functions as an ISG15-specific peptidase, however its catalytic activity is dispensable for controlling IFN signalling. Here, we show that the ISG15-dependent stabilisation of USP18 is necessary but not sufficient for regulation of IFN signalling and that USP18 requires non-covalent interactions with ISG15 to enhance its regulatory function. Intriguingly, this trait has been acquired through co-option of a binding mechanism normally reserved for deISGylation, identifying an unexpected new function for ISG15.

38 **Introduction**

39 The interferon (IFN) response plays a critical role in orchestrating protective antiviral
40 immune responses to combat viral infections (1). Type I IFNs are widely expressed by all
41 nucleated cells following viral infection (2) and signal through the IFN-α/β receptor (IFNAR),
42 which consists of subunits IFNAR1 and IFNAR2 (3). Engagement of IFNAR triggers a
43 phosphorylation cascade involving the reciprocal trans-phosphorylation of Janus kinase 1
44 (JAK1) and tyrosine kinase 2 (Tyk2) (4) and phosphorylation of the cytoplasmic tails of the
45 receptor subunits creating a docking site for the recruitment and subsequent phosphorylation
46 of signal transducer and activator of transcription 1 (STAT1) and STAT2 (5). Once activated,
47 STAT1/2 heterodimers associate with IFN-regulatory factor 9 (IRF9) to form IFN-stimulated
48 gene factor 3 (ISGF3), which binds to the IFN-stimulated response element (ISRE) within the
49 promoters of interferon stimulated genes (ISGs) (1). Several ISGs have been shown to have
50 specific antiviral activity and/or play a role in regulating the IFN response itself. Although this
51 is a prompt and powerful defence against pathogens, a dysregulated type I IFN response can
52 lead to autoinflammatory disease. Therefore, tight regulation of activating and inhibitory
53 signals is of paramount importance for maintaining the protective host-defence nature of the
54 response but limiting tissue damage.

55 ISG15, a ubiquitin-like (UbL) modifier, is synthesised from a precursor that is cleaved
56 at the C-terminus to yield the mature 15-kDa protein with a C-terminal Leu-Arg-Leu-Arg-Gly-
57 Gly (LRLRGG) tail (6,7). ISG15 exists as a free molecule but can also covalently bind to target
58 proteins through the formation of an isopeptide bond between its terminal glycine and the
59 lysine ε-amino group of the target protein (8), a process termed ISGylation (reviewed by
60 (9,10)). ISGylation is reversible through the action of a deISGylase enzyme, the ubiquitin-
61 specific protease 18 (USP18) (11). Independent to its isopeptidase activity on ISG15 (12,13),
62 USP18 interacts with STAT2 to facilitate its recruitment to IFNAR2, where it can inhibit
63 receptor dimerization by interfering with cytoplasmic interactions between IFNAR2 subunits
64 (14–16).

65 Several reports now show that inherited ISG15-deficiency in humans causes type I
66 interferonopathy and autoinflammatory disease (17–19). ISG15-deficient cells exhibited
67 enhanced and prolonged ISG expression and a concomitant resistance to virus infection
68 (18,20,21) a phenotype also associated with USP18 deficiency (13,22). Indeed, despite high
69 levels of *USP18* transcription, USP18 protein levels in ISG15-deficient cells are very low

70 (18,20,21) and previous reports have shown that intracellular ISG15 is required for rescuing
71 USP18 from S-phase kinase associated protein 2 (SKP2)-mediated proteasomal degradation
72 (18,23).
73 Here, we show that, contrary to existing models, the ISG15-dependent stabilisation of
74 USP18 is necessary *but not sufficient* for regulation of type I IFN signalling. Furthermore,
75 independently of ISG15's ability to stabilise USP18, we show that ISG15 and USP18 must
76 interact for USP18 to negatively regulate type I IFN signalling. We find that the C-terminal di-
77 Gly moiety of ISG15 is critical for a stable ISG15-USP18 interaction and we unambiguously
78 demonstrate that abolishing the non-covalent interaction between ISG15 and USP18 results
79 in phenotypes associated with enhanced IFN-α signalling. Together our data illustrates that a
80 binding mechanism normally reserved for deISGylation has been co-opted to serve a crucial
81 role in the fine-tuning of early intracellular immune responses.
82
83

84 **Results**

85

86 **The C-terminal di-Gly motif of ISG15 is important for IFN-α signalling regulation.**

87 In work leading up to this report, we found that reconstituting expression of C-
88 terminal mutants of ISG15, where the terminal di-Gly motif was replaced with di-Ala, in ISG15-
89 deficient cells did not restore the regulation of IFN signalling. To dissect the role of the ISG15
90 C-terminus, we reconstituted expression of Myc-tagged ISG15, which retained its di-Gly motif
91 (ISG15.GG), or C-terminal mutants of ISG15, where the di-Gly motif was either replaced by di-
92 Ala (ISG15.AA) or deleted (ISG15.ΔGG), in our phenotypically validated A549-ISG15$^{-/-}$ cell line
93 (21). To better mimic physiological conditions, reconstituted ISG15 was placed under the
94 control of the native ISG15 promoter (pr15) (Fig. 1A). IFN-α stimulation induced expression
95 of Myc-ISG15 to levels similar to endogenous ISG15 in control A549s and, as expected,
96 ISG15.ΔGG and ISG15.AA did not ISGylate proteins (Fig. 1B). These experimentally tractable
97 cells are therefore valuable for deciphering the role of ISG15 or other ISGs during the innate
98 immune response.

99 We have previously shown that IFN-α treatment of A549-ISG15$^{-/-}$ cells results in
100 enhanced signalling characterised by elevated phospho-STAT1 levels and an augmented and
101 prolonged expression of ISGs (21). Here we determined the ability of C-terminal mutants of
102 ISG15 to regulates signalling. Cells were treated with IFN-α for 30 min, extensively washed,
103 and re-incubated in media without IFN-α. Cell lysates taken immediately after 30-min
104 treatment (0 min) and 30 min later (0.5 h) showed high levels of STAT1 phosphorylation in all
105 tested cell lines (Fig. 1C). Following 24-h treatment with IFN-α, there was evident expression
106 of the ISGs MxA and ISG15, Myc-ISG15 and enhanced expression of STAT1 (Fig. 1C).
107 Interestingly, although phospho-STAT1 levels had declined in A549 control and ISG15.GG-
108 expressing cells at 24 h after IFN-α treatment, levels were clearly higher in A549-ISG15$^{-/-}$ cells
109 and the cells expressing ISG15.AA and ISG15.ΔGG, signifying higher levels of IFN-α signalling
110 in these cells.

111 To confirm these observations at the level of ISG transcripts, cells were treated with
112 IFN-α for 24 h or left untreated. As expected, expression of *MxA* and *HERC5* mRNA was
113 significantly higher in A549-ISG15$^{-/-}$ cells compared to A549 control (2.6- and 3.3-fold
114 respectively, Fig. 1D). Consistent with the phosho-STAT1 levels, ISG mRNA levels were also
115 significantly higher in cells expressing the ISG15.AA and ISG15.ΔGG mutants. Intriguingly, this

116 demonstrated a gradient pattern of regulation where ISG15.GG-expressing cells regulated
117 similar to control A549 cells, cells expressing the ISG15.AA mutant were characterised by
118 higher ISG levels similar levels to A549-ISG15$^{-/-}$ cells, but cells expressing the ISG15.ΔGG
119 mutant consistently showed a trend towards an intermediate level of regulation. No
120 significant difference was observed between the ISG15.GG-expressing cells and the control,
121 suggesting that the level of ISG15 expression in this system is sufficient to regulate IFN
122 signalling similarly to unmodified control cells (Fig. 1D). Overall, these data show that the C-
123 terminal di-Gly motif is important for the negative regulation of type I IFN signalling.
124
125 **Quantitative analysis of global protein abundance shows enhanced IFN-α immune**
126 **responses demonstrates the importance of the ISG15 C-terminus for regulation.**
127 Next, we employed a multiplexed proteomic approach to obtain an unbiased, global
128 picture of the proteomic changes induced by IFN-α across our cell lines and to begin to tease
129 out the processes that could underpin interferonopathies. Cells were treated with IFN-α for
130 24, 48 or 72 h, and whole cell protein abundance measured using 16-plex TMT labelling and
131 MS3 mass spectrometry (Fig. 2A). In total, 7112 proteins were quantified (full data can be
132 visualised using the 'Plotter' in Supplementary File 1). As expected, the abundance of IFN-
133 stimulated proteins, such as ISG20 and IFIT1 was higher in the A549-ISG15$^{-/-}$ and ISG15.AA-
134 expressing cells compared to the A549 control and ISG15.GG-expressing cells (Fig. 2B). To
135 determine whether this trend was reflected more generally, ISGs were identified by (a)
136 comparison to the Interferome database, and (b) stringent criteria to identify proteins
137 upregulated by IFN-α compared to mock treatment in A549 control cells (>1.7-fold increase
138 in abundance, Fig. 2C). Ninety proteins identified by these criteria as interferon stimulated
139 were expressed at significantly higher levels by A549-ISG15$^{-/-}$ and ISG15.AA cells compared to
140 both A549 control and ISG15.GG cells (Fig. 2C). As expected, there was no statistically
141 significant difference in ISG expression between A549 control and ISG15.GG-expressing cells,
142 providing further evidence that genetic manipulation did not cause any inadvertent
143 phenotypic changes to the cells.
144 To determine whether specific pathways were enriched in the ISG15$^{-/-}$ and ISG15.AA
145 cells, we used DAVID analysis to examine proteins upregulated >1.7-fold compared to control
146 A549 cells. As anticipated, effector molecules involved in cellular immune responses, such as
147 innate immunity and antiviral defence, were enriched in all tested cell lines with several

148 overlapping factors in each cluster (Fig. 2D). Although fewer pathways were enriched in
149 ISG15.GG cells suggesting tighter control than in cells expressing C-terminal mutants, antiviral
150 defense, immunity and innate immunity pathways were identified suggesting that their
151 control was not as tightly regulated compared to control A549 cells. This might be because,
152 despite being inducible by IFN-α, lentivirally-delivered ISG15 transgenes are not in their
153 authentic genomic loci and therefore expression is affected. Interestingly, components of IFN-
154 γ mediated signalling and antigen processing and presentation pathways were selectively
155 enriched in A549-ISG15$^{-/-}$ and ISG15.AA-expressing cells, for example transporter associated
156 with antigen presentation 1 (TAP1) (Fig. 2D-E). One potential explanation is the selective
157 enrichment in these cells of key regulatory factors induced by primary IFN-γ signalling (24,25),
158 such as the interferon-regulatory factor 1 (IRF1) whose expression is induced by STAT1
159 homodimers typical of IFN-γ-induced ISGs with gamma-activated sequences (GAS) in their
160 promoters and not STAT1-STAT2-IRF9 (ISGF3) complexes that characteristically induce genes
161 with IFN-stimulated response elements (ISRE) activated by type I IFN signalling (although GAS
162 genes can be activated upon type I IFN signalling as concentrations of STAT1-homodimers
163 increase; Fig. 2E). It may be that enrichment with components of IFN-γ signalling derives
164 through the enhanced levels of active STAT1 (Fig. 1C) and subsequent increased stoichiometry
165 of STAT1 homodimer complexes in ISG15$^{-/-}$ and ISG15.AA cells, leading to gene expression
166 through binding to GAS elements in the promoters of ISGs (26). Moreover, cell cycle
167 components and several factors with nucleotide binding properties were also enriched in cells
168 with a dysregulated IFN-α signalling response (Fig. 2D). In conclusion, using unbiased
169 proteomic analyses, we have further confirmed that the C-terminal di-Gly domain of ISG15 is
170 important for regulation of type I IFN responses. It is also possible that pathways associated
171 with IFN-γ, which include genes associated with antiproliferative phenotypes and apoptosis,
172 may underpin the pathogenesis of autoinflammatory diseases associated with loss of type I
173 IFN signalling control.
174
175 **IFN-α-pretreatment leads to viral resistance in cell lines expressing the C-terminal mutants,**
176 **ISG15.AA and ISG15.ΔGG.**
177 We and others have previously shown that pre-treatment of ISG15-deficient cells with
178 IFN-α renders them resistant to viral infection (20,21). Because we have reported that viral
179 resistance in ISG15-deficient cells is directly related to dysregulated type I IFN signalling (21),

180 this assay serves as an excellent model for investigating the biological implications of ISG15
181 loss-of-function and the regulatory role of the ISG15 di-Gly motif. Cell lines were primed with
182 IFN-α for 18 h, then infected with a recombinant parainfluenza virus type 5 (PIV5) expressing
183 mCherry (rPIV5-mCherry). Because the PIV5 V-protein targets STAT1 for proteasomal
184 degradation, rPIV5-mCherry can replicate in A549 control cells despite a primed IFN response,
185 albeit with reduced kinetics (27). By 48 h of infection in A549 control cells, there was a
186 corresponding increase in PIV5 NP expression, STAT1 was undetectable and MxA expression
187 was reduced (Fig. 3A). As anticipated, pretreatment with IFN-α rendered A549-ISG15$^{-/-}$ cells
188 resistant to PIV5 infection, whereas reconstituted expression of ISG15.GG reversed the
189 phenotype (Fig. 3A,B). Interestingly, like A549-ISG15$^{-/-}$ cells, NP expression was undetectable
190 at 24 h post-infection in both ISG15.AA and ISG15.ΔGG-expressing cells (Fig. 3A). Although
191 PIV5 infection recovered to some extent by 48 h, NP expression was still significantly reduced
192 by 90% and 45% at 48 h p.i. in cells expressing ISG15.AA and ISG15.ΔGG, respectively (Fig. 3B).
193 Intriguingly, this gradient in viral protein expression inversely correlated with the gradient
194 observed for ISG expression (Fig. 1D), linking the ability of ISG15 and ISG15 mutants to
195 regulate the magnitude of the antiviral response with their capacity to support infection.
196 Moreover, we used fluorescence microscopy to visualise mCherry expression and indicate
197 rPIV5-mCherry replication. Consistent with NP expression, no mCherry was detected in the
198 A549-ISG15$^{-/-}$ cells, with low or moderate levels in cells expressing the ISG15.AA and
199 ISG15.ΔGG mutants, respectively (Fig. 3C). Altogether, these experiments highlight the impact
200 on viral infection of the C-terminal di-Gly motif of ISG15, via its regulation of IFN signalling.
201

202 **The ISG15-dependent stabilisation of USP18 is necessary but not sufficient for the**
203 **regulation of IFN signalling.**

204 It has been established that ISG15 is crucial for sustaining the levels of USP18, a key
205 negative regulator of IFN signalling, by preventing its SKP2-mediated ubiquitination and
206 proteasomal degradation (18,20,23). Therefore, we reasoned that modifications to the ISG15
207 C-terminus might have affected its ability to stabilise USP18. To test this, cells were treated
208 with IFN-α for 24 and 48 h and cell lysates were subjected to immunoblot analysis.
209 Remarkably, although USP18 expression was dramatically reduced in A549-ISG15$^{-/-}$ cells, its
210 expression in ISG15.AA and ISG15.ΔGG expressing cells were comparable to levels observed
211 in ISG15.GG-expressing and control A549 cells (Fig. 4A). The proteomics analysis described in

212 Fig. 2 provided independent verification that ISG15 expression, independently of its ability to
213 regulate signalling, was able to stabilise USP18 (Fig. 4B). Taken together, these experiments
214 clearly show that, although the stabilization of USP18 is crucial, it is not sufficient for the
215 regulation of type I IFN signalling.
216
217 **The C-terminal di-Gly motif of ISG15 is required for the ISG15-USP18 interaction.**
218 Because neither ISGylation (18,21) or ISG15-dependent stabilisation of USP18 are
219 sufficient for the regulation of type I IFN signalling, the mechanism of ISG15 action with
220 respect to the IFN pathway is likely to involve a non-covalent protein-protein interaction. The
221 most likely candidate is USP18, given that during the deISGylation process, USP18
222 deconjugates ISG15 from target substrates in a process that requires engagement of USP18's
223 catalytic triad with the C-terminal tail LRLRGG of ISG15 (28,29). We therefore assessed the
224 ability of endogenous USP18 to interact with ISG15 and its C-terminal mutants in our
225 reconstituted cell lines. Myc-tagged ISG15 was immunoprecipitated from ISG15-
226 reconstituted cells following a 24-h IFN-α treatment. To verify that ISGylation was not
227 necessary for the interaction between ISG15 and USP18, we knocked-out UBA7 (E1 enzyme
228 essential for ISGylation) from our ISG15.GG-expressing cells by CRISPR/Cas9 genome editing
229 (Fig. 5). Here we show that the ability of ISG15 mutants to bind USP18 mirrored the gradient
230 pattern of ISG mRNA regulation (Fig. 1D) and corresponding effects on viral infection (Fig. 3).
231 Reconstituted ISG15.GG efficiently bound USP18; however, the ISG15.AA mutant was unable
232 to interact with USP18, whereas ISG15.ΔGG did interact but at reduced levels compared to
233 ISG15.GG (Fig. 5). Notably, USP18 co-immunoprecipitated with ISG15.GG in UBA7$^{-/-}$ cells,
234 confirming that the ISG15-USP18 interaction is not dependent on ISGylation (Fig. 5).
235 Furthermore, we noted that all forms of ISG15 stabilised USP18 (see WCL samples, Fig. 5
236 lower panels), again confirming that ISG15 stabilised USP18 independently of their ability to
237 regulate signalling and to add to this, stability is not dependent on their interaction.
238 Collectively, these results indicate that the C-terminal di-Gly motif is important for ISG15-
239 USP18 interaction and that non-covalent binding of ISG15 and USP18 is necessary to facilitate
240 USP18's inhibition of type I IFN signalling.
241
242 **The ISG15-USP18 interaction is important for the tight regulation of IFN-α signalling.**

243 To independently assess the requirement of the ISG15-USP18 interaction for the
244 regulation of IFN signalling, we mutated the USP18 isoleucine residue at position 60
245 (USP18.I60N), which is known to abolish interactions with ISG15 (23). In addition, since
246 previous studies have shown that the mouse Usp18 (Ubp43) negatively regulates IFN
247 signalling in the absence of its isopeptidase activity (13), we additionally investigated the
248 catalytically inactive human mutant USP18.C64S. We first sought to evaluate the impact of
249 these point-mutations on ISG15-USP18 binding by coimmunoprecipitation (co-IP) (Fig. 6A).
250 Consistent with previous studies (23), our data demonstrated that the USP18.I60N mutant
251 was unable to interact with ISG15.GG, whereas the USP18.C64S mutant had stronger binding
252 affinity for ISG15 compared to wt USP18 (23) (Fig. 6A).
253 Next, we asked whether the USP18.I60N mutant could still be recruited to the IFNAR2
254 signalling complex despite its inability to interact with ISG15. Previous studies have shown
255 that STAT2 recruits USP18 to the IFNAR2 receptor, where it interferes with the cytosolic
256 interactions between the type I IFN receptor subunits (13,16,30). We co-expressed a V5-
257 tagged version of the IFNAR2 cytosolic domain (aa 265-515) and Myc-tagged STAT2 with Flag-
258 tagged wt USP18, USP18.I60N or USP18.C64S in HEK293T cells and performed co-IP assays
259 using anti-V5 antibody coupled to protein G Dynabeads (Fig. 6B). As expected, the IFNAR2
260 cytoplasmic domain interacted with STAT2 and wt USP18 (Fig. 6B). Intriguingly, both mutant
261 forms of USP18 co-immunoprecipitated with the IFNAR2 receptor subunit (Fig. 6B),
262 demonstrating that neither the I60N or C64S point mutations disrupted the recruitment of
263 USP18 to the receptor or the subsequent formation of the USP18-dependent type I IFN
264 receptor inhibitory complex.
265 In order to evaluate the functional consequences of these point mutants, we used
266 CRISPR/Cas9 genome editing to knock-out USP18 gene expression in A549 cells, as described
267 before (21), followed by lentiviral transduction to reconstitute inducible expression of Flag-
268 tagged wt or mutant forms of USP18 in the A549-USP18$^{-/-}$ cell line (Fig. 6C). To evaluate USP18
269 expression, A549 NC1-control cells, which express a negative control guide RNA (NC1) that is
270 nontargeting in humans, A549-USP18$^{-/-}$ and USP18-reconstituted derivatives were treated
271 with IFN-α for 48 h and cell lysates were subjected to immunoblot analysis (Fig. 6D).
272 Interestingly, the expression levels of the reconstituted forms of USP18 were higher
273 compared to NC1 control (Fig. 6D), perhaps because expression of reconstituted USP18 was
274 driven by the ISG15 promoter, which is strongly IFN-responsive (31), instead of its native

275 promoter. Consistent with previous observations (13), knockout of USP18 increased the levels
276 of ISG15 conjugates, whereas unexpectedly, reconstitution of wt USP18 resulted in a lower
277 level of ISGylation compared to the NC1 control cells. The expression of USP18.I60N mutant
278 was higher compared to the expression levels of wt USP18 and USP18.C64S; however, the
279 accumulation of ISGylated proteins was only marginally increased compared to the cell line
280 expressing wt USP18 (Fig. 6D). Interestingly, protein expression of ISGs, ISG15 and MxA,
281 appeared to be elevated in A549-USP18$^{-/-}$ and the USP18.I60N-expressing cells, signifying
282 higher levels of JAK/STAT signalling (Fig. 6D). As anticipated, expression of the catalytically
283 inactive mutant USP18.C64S resulted in higher levels of ISGylated proteins compared to the
284 cell line reconstituted with wt USP18 (Fig. 6D), and, similar to its mouse counterpart
285 (UBP43.C61S) (13), resulted in lower ISG15 protein expression compared to wt USP18. These
286 observations indicate a dysregulation of the IFN response in an isopeptidase-independent
287 manner (Fig. 6D).

288 To further evaluate the importance of ISG15-USP18 binding in the regulation of IFN-α
289 signalling, as described in Fig. 1D, we measured the levels of *MxA* and *HERC5* gene expression
290 in these cells (Fig. 7A). Remarkably, *MxA* and *HERC5* expression was significantly higher in
291 USP168.I60N-expressing derivatives compared to NC1 control (averaging around 2.5-fold),
292 denoting that the lack of ISG15-USP18 interaction in these cells led to a dysregulated IFN
293 response, a phenotype similar to A549-USP18$^{-/-}$ cells (Fig. 7A). Notably, ISG expression levels
294 in cells expressing the USP18.C64S mutant were consistently lower than, but not significantly
295 different to, NC1 control cells.

296 We predicted that the elevated expression of ISGs in USP18.I60N-expressing cells
297 would engender resistance to infection. Using the assay described in Fig. 3, we observed that
298 IFN-α-pretreated USP18.I60N-expressing cells were largely resistant to infection, as similar to
299 A549-USP18$^{-/-}$ cells, expression of PIV5 NP was barely detectable (Fig. 7B). Quantitative
300 analysis of NP expression levels showed that viral replication was reduced more than 95% in
301 IFN-α-pretreated A549-USP18$^{-/-}$ and USP18.I60N-expressing cells, whereas the levels of viral
302 infection in cell lines expressing the wt and the catalytically inactive mutant USP18.C64S were
303 similar to NC1 control, confirming regulation in these cells (Fig. 7C). mCherry expression levels
304 further verified that IFN-α-pretreatment constrained virus replication in A549-USP18$^{-/-}$ and
305 USP18.I60N-expressing cells (Fig. 7D). Altogether, these experiments demonstrate that
306 disruption of the ISG15-USP18 interaction enhances IFN-mediated signalling, suggesting that

307 ISG15 plays a crucial role in the negative regulation of IFN signalling beyond its indirect
308 function as a USP18 stabiliser.
309
310 **The ISG15-USP18 interaction is important for the IFN-α-induced desensitization of IFN-α**
311 **signalling.**
312 Previous studies have shown that USP18 is crucial for the IFN-α-induced
313 desensitization of IFN-α signalling by disrupting the recruitment of IFNAR1 into the ternary
314 IFN-α-IFNAR1-IFNAR2 complex, decreasing the activation of signalling (15,16,30,32). To test
315 whether the ISG15-USP18 interaction is important for this USP18-dependent negative
316 regulation of IFN receptor plasticity, we established a desensitization assay based on previous
317 reports (15), where A549 NC1-control cells, A549-USP18$^{-/-}$ and USP18-reconstituted
318 derivatives were primed with IFN-α for 8 h or left untreated, washed extensively and then
319 maintained in medium without IFN for 16 h. During the prime-rest phase, USP18 is expressed
320 and prevents further signalling activation following additional stimulation. Following the 16-
321 h resting period, cells were stimulated with IFN-α for 30 min and cell lysates were subjected
322 to immunoblotting to assess phosho-STAT1 expression, which is indicative of early activation
323 of IFN signalling (Fig. 8A). As expected, priming with IFN-α decreased the responsiveness of
324 NC1-control cells to subsequent IFN stimulation as similar levels of phosho-STAT1 were
325 detected in primed and non-primed control cells. A similar phenotype was observed in A549-
326 USP18$^{-/-}$ cells reconstituted with wt USP18 or the catalytically inactive mutant USP18.C64S,
327 indicating that the sensitivity of these cells to IFN-α was downregulated following priming
328 with IFN-α (Fig. 8A). Consistent with previous reports (15), A549-USP18$^{-/-}$ cells were not
329 desensitized to IFN-α resulting to 3.8-fold increase in STAT1 phosphorylation when primed
330 with IFN-α compared to the non-primed control (Fig. 8B). Remarkably, cells expressing the
331 USP18.I60N mutant retained their responsiveness toward IFN-α similar to A549-USP18$^{-/-}$ cells
332 (Fig. 8A). Specifically, STAT1 phosphorylation in USP18.I60N-expressing cells showed 3.2-fold
333 increase following IFN-α priming compared to the non-primed control (Fig. 8B). Overall, our
334 data strongly suggest that the ISG15-USP18 interaction is important for the USP18-dependent
335 regulation ternary IFNAR complexes.
336

337 **Discussion**

338 The negative regulation of the type I IFN system is controlled at multiple levels by a
339 variety of mechanisms, involving sequestration of effector molecules and post-translational
340 modifications, such as ubiquitination or dephosphorylation (reviewed by Arimoto et al (33)).
341 Humans with ISG15-deficiency display abnormally strong type I IFN immunity highlighting the
342 emerging role of ISG15 as a central regulator of immunity (17,18,21,23). Current models
343 suggest that ISG15 antagonizes the SKP2-mediated ubiquitination and degradation of USP18,
344 promoting its functions (18,20,23). We extend these findings and show that the ISG15-
345 dependent stabilisation of USP18 is necessary *but not sufficient* to regulate IFN-I signalling
346 and that non-covalent binding of ISG15 and USP18 is also necessary to facilitate USP18's
347 inhibitory function (Fig. 9). Intriguingly, this is achieved through co-option of a binding
348 mechanism normally reserved for deISGylation and identifies an unanticipated new function
349 for the UbL ISG15.

350 It is well known that the conserved C-terminal di-Gly motif of ISG15 is essential for
351 ISGylation (34,35); therefore, the ISGylation-deficient mutants, ISG15.AA and ISG15.ΔGG,
352 have been extensively used for exploring the functional consequences of ISGylation. Here, we
353 have reported that the ISG15 C-terminal mutants display different propensities for binding
354 USP18 but, despite this, both mutants stabilize USP18 to levels comparable to wt ISG15 (Fig.
355 4). Although not having been previously assessed in the context of an IFN response, this is
356 consistent with previous reports showing that ISG15 can abrogate the USP18-SKP2 complex
357 and rescue USP18 from proteasomal degradation independent of its ability to bind USP18
358 (23). Importantly, our work strongly suggests that ISG15-USP18 binding is required for USP18-
359 dependent regulation of the type I IFN response as the level of binding to USP18 faithfully
360 reflected the level of IFN-α signalling regulation and the permissiveness of cells to viral
361 infection. We independently confirmed the importance of a ISG15-USP18 interaction as
362 expression of mutant USP18 unable to bind ISG15 (USP18-I60N) could not regulate type I IFN
363 signalling even though it could interact with the IFNAR2 signalling complex (Fig. 6). In line with
364 findings using mouse Usp18 (12,13), the protease activity of human USP18 remains
365 dispensable for signalling regulation in humans.

366 Previous studies have shown that USP18 desensitises type I IFN signalling (14–16).
367 Specifically, STAT2 recruits USP18 to the IFNAR2, where it interferes with the cytosolic
368 interactions between receptor subunits, impeding the recruitment of IFNAR1 into the ternary

369 complex (14,16). Remarkably, we demonstrate here that the non-covalent binding of ISG15
370 and USP18 is required for the USP18-dependent negative regulation of IFNAR dimerization
371 (Fig. 8). Consistent with previous reports (14), our data show that ISG15 appears dispensable
372 for the interaction of USP18 IFNAR2; therefore, we hypothesize that the ISG15's contribution
373 may be essential for further stabilizing the USP18-inhibitory complex, or for recruiting further
374 not yet identified interaction partners of USP18 or perhaps promoting a conformational
375 change in USP18 necessary for its inhibitory activity.

376 Structural studies have shown that the ISG15-bound USP18 adopts a different
377 structural confirmation, where the 'switching loop' in the thumb domain of USP18 acquires
378 an active conformation, enabling access of the LRLRGG C-terminal tail of ISG15 into the
379 catalytic cleft (28,29). Here, we showed that replacing the C-terminal di-Gly of ISG15 with di-
380 Ala completely abolishes ISG15-USP18 interaction (Fig. 5). Although this amino acid
381 substitution is considered subtle, it is possible that the two extra methyl groups present in
382 the di-Ala motif are not accessible to the tight catalytic cleft of USP18, abolishing the
383 interaction with the ISG15.AA mutant. This may also explain why the ISG15.ΔGG mutant,
384 which retains the LRLR peptide of the C-terminal tail, interacted to a greater extent with
385 USP18 compared to ISG15.AA. Moreover, in line with previous findings (23), we showed that
386 the USP18.I60N mutant was unable to bind ISG15 (Fig. 6A). Interestingly, Ile residue 60 does
387 not belong to the ISG15-binding boxes (28) but its proximity to the catalytic cysteine (C64)
388 may affect the conformational dynamics of the catalytic cleft, diminishing the interaction with
389 ISG15. Consistent with previous reports (23), we have observed that the catalytically inactive
390 mutant (USP18.C64S) has stronger binding affinity for ISG15, compared to wt USP18, and
391 there is a consistent pattern of stronger negative regulation (lower ISG expression, increased
392 desensitization to IFN-α) in cells expressing this mutant, supporting our observation that the
393 level of binding of ISG15 toward USP18 determines the level of IFN-α signalling regulation.
394 Hence, it is possible that the binding of ISG15 locks USP18 into a more stable structural
395 confirmation that may serve its regulatory functions at the level of IFNAR assembly. A caveat
396 to this model is that Isg15 is dispensable for Usp18-mediated regulation of type I IFN signalling
397 in mice (20).

398 That Isg15 does not stabilise Usp18 in mice (20), illustrates interesting interspecies
399 variation with regard to ISG15 function. Unlike the highly conserved ubiquitin (36), ISG15
400 possesses remarkable sequence variation between species, with sequence identity around

401 70% between human and mouse genes, suggesting that the different biochemical properties
402 of ISG15 between species may be key determinants of ISG15's species-specific functions
403 (37,38). Indeed, it has been shown that human ISG15 associates with higher affinity to USP18
404 compared to its mouse counterpart (20), which in agreement with our findings, suggests that
405 gain-of-function mutations in ISG15 and/or USP18 that facilitate stronger ISG15-USP18
406 interactions have been evolutionary selected in humans. Why this trait is apparent in humans
407 and not mice is of interest and may suggest that an additional, yet-to-be identified factor is
408 taking the place of ISG15 in mice, or that humans may require a different level of IFN-
409 regulatory control.

410 Intriguingly, our proteomics profiling and pathway analyses highlighted the
411 enrichment of components involved in IFN-γ signalling in A549-ISG15$^{-/-}$ and ISG15.AA-
412 expressing cells (Fig. 2). This may be due to the accumulation of STAT1 homodimers as a by-
413 product of enhanced type I immunity, leading to enrichment of GAS-containing genes
414 (24,25,39), such as IRF1 and MHC Class I proteins in these cells. IRF1 transcription factor itself
415 is involved in the regulation of genes implicated in antiproliferative (40) and antigen
416 processing pathways (41–43). These findings support our previous work that demonstrates
417 that ISG15 deficiency leads to translational regression following IFN-α treatment (21) and
418 further suggest that intervention strategies that target the ISG15-USP18 interaction may be
419 of therapeutic use in anticancer therapy.

420 In conclusion, we have demonstrated that intracellular ISG15 is essential to negatively
421 regulate IFN-α responses via its non-covalent interaction with USP18, thereby averting
422 autoinflammatory consequences of uncontrolled type I IFN signalling. This hitherto human-
423 specific trait has been acquired through co-option of a binding mechanism normally reserved
424 for the process of deISGylation. Further investigation is needed to decipher the biophysical
425 properties of the USP18-mediated inhibitory complex at the level of IFNAR assembly and
426 resolve how the binding of ISG15 to USP18 facilitates those interactions.
427
428
429
430
431

432 **Methods**

433 **Cells**

434 HEK293T (human embryonic kidney cell), A549 cells (human adenocarcinoma alveolar
435 basal epithelial cells), and derivatives, were were grown as monolayers in Dulbecco's
436 modified Eagles's medium (DMEM; Sigma) supplemented with 10% (v/v) foetal bovine serum
437 (FBS, Biowest) and incubated in 5% (v/v) $CO_2$ at 37°C in a humidified incubator.A549-ISG15$^{-/-}$
438 cells (clone B8) were generated as previously described using CRISPR/Cas9n system;
439 transfectants were enriched by treating cells with puromycin (1 µg/ml) for 2 days, then single-
440 cell cloned and successful knockout cells were validated by immunoblot analysis (21).
441 Lentiviral technology was used to reconstitute expression of wt ISG15.GG (NCBI Ref Seq,
442 NM_005101.3) or C-terminal mutants, ISG15.AA and ISG15.ΔGG in A549-ISG15$^{-/-}$ to generate
443 the following derivative cell lines; A549-ISG15$^{-/-}$:prI5-GG, A549-ISG15$^{-/-}$:prI5-AA, A549-ISG15$^{-}$
444 $^{/-}$:prI5-ΔGG, respectively. Expression of wt and C-terminal mutant forms of ISG15 was driven
445 by the native ISG15 promoter (pr15) (NCBI Ref seq, NG_033033.2) cloned using our lentiviral
446 vector. An internal ribosome entry site (ISRE) downstream the ISG15 gene allows expression
447 of puromycin resistance (pac) gene following induction of pr15. Hence, for puromycin
448 selections, cells were primed with 1000 IU/ml IFN-α for 4 h prior treatment with puromycin
449 (1 µg/ml) for 2 days. To generate the A549-ISG15$^{-/-}$:UBA7$^{-/-}$:pr15-GG cell line, A549-ISG15$^{-/-}$
450 :pr15-GG cells were further modified to stably express *Streptococcus pyogenes* Cas9 and then
451 transduced with UBA7 sgRNA-expressing lentiGuide-Puro (sgRNA sequences; sense:
452 caccGCACACGGGTGACATCACTG; antisense: aaacCAGTGATGTCACCCGTGTGC) as described
453 previously (21). For generating A549-USP18$^{-/-}$ cell lines, A549 cells were modified to stably
454 express *Streptococcus pyogenes* Cas9 and then transduced with USP18 sgRNA-expressing
455 lentiGuide-Puro (sgRNA sequences; sense: caccgGGGGCCGCACTGCTTTCTGC; antisense:
456 aaacGCAGAAAGCAGTGCGGCCCCc). Blasticidin/puromycin-resistant A549-USP18$^{-/-}$ cells were
457 single-cell cloned in 96-well plates and successful knockout cells were validated by
458 immunoblot analysis. Lentiviral technology using our pr15 lentiviral vector was used to
459 reconstitute expression of wt USP18 (NCBI Ref seq NM_017414.4) or the point mutants
460 USP18.I60N and USP18.C64S (generated by site-directed mutagenesis) in A549-USP18$^{-/-}$ to
461 generate the A549-USP18$^{-/-}$:prI5-USP18.wt, A549-USP18$^{-/-}$:prI5-USP18.I60N and A549-USP18$^{-}$
462 $^{/-}$:prI5-USP18.C64S, respectively. All lentiviruses used in this study were generated in

463 HEK293T cells using a previously described self-inactivating lentiviral constitutive expression
464 system (44).
465
466 **Reverse transcription quantitative PCR**
467 To measure ISG expression levels, cells were treated with 1000 IU/ml IFN-α for 18 h and
468 intracellular total RNA was isolated with TRIZOL (ThermoFisher Scientific) and Direct-zol RNA
469 Miniprep Plus kits (Zymo Research), including removal of contaminating DNA following DNase
470 I treatment, following the manufacturer's instructions. A total of 500 ng of RNA was reverse
471 transcribed using LunaScript® reverse transcriptase (New England Biolabs) according to the
472 manufacturer's recommendations. Quantitative PCRs (qPCRs) were performed with PerfeCTa
473 SYBR green SuperMix (Quanta BioScience) using fast two-step cycling performed in a
474 Mx3005P real time PCR machine (Stratagene) and included an initial 2 min enzyme activation
475 step at 95°C, followed by 40 cycles of 5 s at 95°C and 20 s at 60°C. Melting curve analysis was
476 performed to verify amplicon specificity. For each assay, quantification of *β-ACTIN* mRNA was
477 used to normalize between samples and the average cycle threshold (CT) was determined
478 from three independent cDNA samples from independent cultures (technical replicates). Fold
479 changes were determined from three independent assays performed at different times
480 (biological replicates). Relative expression compared to non-treated control cells was
481 calculated using the ΔΔCT method. Primer sequences were: *MxA*
482 5'GCCTGCTGACATTGGGTATAA and 5'CCCTGAAATATGGGTGGTTCTC, *HERC5*
483 5'GACGAACTCTTGCACCGTCTC and 5'GCGTCCACAGTCATTTTCCAC, *β-ACTIN*
484 5'AGCGAGCATCCCCCAAAGTT and 5'AGGGCACGAAGGCTCATCATT.
485
486 **Viral infections and IFN treatment**
487 Recombinant mCherry-expressing parainfluenza virus type 5 (rPIV5-mCherry)
488 (provided by Professor Biao He, University of Georgia) (45) stocks were prepared by
489 inoculating Vero cells at a multiplicity of infection (MOI) of 0.001 with continual rocking at
490 37°C. Supernatants were harvested at 2 d p.i., clarified by centrifugation at 3,000 x g for 15
491 min, aliquoted and snap frozen. Titres were estimated by standard plaque assay on Vero cells
492 in 6-well plates.
493 For virus resistance assays, cell monolayers at 70-80% confluency were infected in 6-
494 well plates with virus diluted in 1 ml media supplemented with 2% (v/v) FBS to achieve an

495 MOI of 10. Virus adsorption was for 1 h with continual rocking at 37°C, after which 1 ml of
496 media supplemented with 2% (v/v) FBS was added to the viral inoculum and incubated in 5%
497 (v/v) $CO_2$ at 37°C until harvested. When cells were treated with IFN-α prior to infection (pre-
498 treated) this was done with 1000 IU/ml IFN-α2b (referred to as IFN-α from here on; IntronA,
499 Merck Sharp & Dohme Ltd). IFN-α remained on cells for the duration of experiments. Cells
500 were either processed for immunoblot analysis or observed with fluorescence microscopy
501 using EVOS M5000 Imaging System (pictures taken at 10X magnification).
502
503 **Immunoblotting**
504 Confluent monolayers in 6-well dishes were lysed with 250 µl 2 x Laemmli sample
505 buffer (4% w/v SDS, 20% v/v glycerol, 0.004% w/v bromophenol blue and 0.125 M Tris-HCl,
506 pH 6.8 with 10% v/v β-mercaptoethanol) for 10 min, incubated at 95°C for 10 min, sonicated
507 at 4°C with 3 cycles of 30 s on 30 s off in a Bioruptor Pico (Diagenode) and clarified by
508 centrifugation at 12,000 x g, 4°C for 10 min. SDS-PAGE in Tris-glycine-SDS running buffer and
509 immunoblotting followed standard techniques using the following antibodies: mouse
510 monoclonal anti-ISG15 F-9 (Santa Cruz Biotechnology Cat# sc166755), rabbit polyclonal anti-
511 ISG15 H-150 (Santa Cruz Biotechnology Cat# sc50366), rabbit polyclonal anti-MxA
512 (Proteintech Cat# 13750-1-AP), mouse monoclonal anti-UBA7 (anti-UBE1L B-7; Santa Cruz
513 Biotechnology Cat# sc-390097), rabbit anti-USP18 (Cell Signalling Technology Cat# 4813S),
514 mouse monoclonal anti-total STAT1 (N-terminus; BD Transduction Laboratories™ Cat#
515 610116), rabbit monoclonal anti-phosphorylated STAT1 (anti-phospho-STAT1 (Tyr701); Cell
516 Signalling Technology Cat# 9167), mouse monoclonal anti-PIV5 NP 125 (46), mouse anti-V5
517 tag Pk 336 (46), antibody mouse monoclonal anti-β-actin (Sigma Cat# A2066). For quantitative
518 immunoblots primary antibody-probed membranes were incubated with IRDye secondary
519 antibodies (LiCOR) and signals detected using an Odyssey CLx scanner. Data were processed
520 and analysed using Image Studio software (LiCOR).
521
522 **Immunoprecipitation**
523 Prior immunoprecipitation, HEK293T cells were transiently transfected to express the
524 proteins of interest using calcium-phosphate coprecipitation transfections. One day prior to
525 transfection, HEK293T cells were seeded in 6-well plates such that they are logarithmically
526 growing on the day of transfection (i.e., 50-60% confluent). A total of 200 µl calcium-

527 phosphate precipitate was prepared for each well by mixing each plasmid DNA (diluted in
528 total 90 µl in $dH_2O$) with 10 µl of 2.5M $CaCl_2$ solution. DNA/$CaCl_2$ solutions were added
529 dropwise into 100 µl of 2× HEPES-buffered saline (HeBS) (50 mM HEPES, 0.28 M NaCl, 10 mM
530 KCl, 1.5 mM $Na_2HPO_4$, 12 mM D-glucose, pH 7.05) and incubated for 20 min at room
531 temperature (RT). Chloroquine diphosphate solution was added to cell culture media to 25
532 µM final concentration and calcium phosphate precipitate was added dropwise onto plate
533 and mixed gently. At 16 h after transfection, the calcium phosphate precipitate was removed,
534 and cells were incubated for further 24 h before subjected to co-immunoprecipitation (co-IP)
535 assays. The following vectors were used for co-IP assays: pLHCX-STAT2-Myc (kind gift from Dr
536 Michael Nevels, St Andrews University), pcDNA3.1-USP18.wt-3XFlag, pcDNA3.1-USP18.I60N-
537 3XFlag, pcDNA3.1-USP18.C64S-3XFlag, pcDNA3.1.ISG15.GG and pcDNA3.1-IFNAR2.CTD-V5,
538 which expresses the cytoplasmic C-terminal domain (CTD) of IFNAR2.
539 For co-IP assays, confluent monolayers of IFN-treated A549 derivatives grown in T150
540 $cm^2$ flasks or plasmid-transfected HEK293T cell cultures grown in 6-well plates were harvested
541 in phosphate-buffered saline (PBS), pelleted by centrifugation (300 × g, 5 min, 4°C) and
542 resuspended in 1 ml co-IP lysis buffer (50 mM Tris pH 7.5, 150 mM NaCl, 0.1% [v/v] Triton-X)
543 supplemented with 1x cOmplete™ protease inhibitor cocktail (Merck). The supernatant was
544 separated by centrifugation (12,000 x g, 10 min, 4°C) and incubated overnight at 4°C with
545 gentle rotation with 40 µl Pierce Anti-c-Myc Magnetic Beads (ThermoFisher Scientific Cat#
546 88842) or anti-Flag® M2 Magnetic Beads (Merck Cat# M8823) or anti-V5 tag antibody coupled
547 with Protein G Dynabeads™ (Invitrogen) by following manufacturer's instructions. Complexes
548 were washed three times with co-IP wash buffer (1X TBS; 50 mM Tris pH 7.5, 150 mM NaCl),
549 incubated in 50 µl 1X NuPage LDS sample buffer (ThermoFisher Scientific) for 20 min at RT
550 and then, further incubated for 10 min at 70°C. Beads were magnetically separated and 10%
551 (v/v) of β-mercaptoethanol was added in the eluted supernatant containing target antigens.
552 Immunoprecipitates were subjected to SDS-PAGE and immunoblotting.
553
554 **Desensitization assay.**
555 Cells grown to 70-80% confluency in 6-well plates were primed with 2000 IU/ml IFN-
556 α (equivalent to 20 ng/ml) for 8 h or left untreated. Following priming, cells were washed four
557 times with PBS and maintained in medium without IFN for 16 h (resting period) and then

558 stimulated with 2000 IU/ml IFN-α for 30 min. Cell lysates were subjected to SDS-PAGE and
559 immunoblotting.
560
561 **Tandem mass tags (TMT)-based quantitative proteomics**
562 Tandem mass tags (TMT)-based proteomics was used to quantify differences in
563 protein abundance following IFN-α treatment in A549 control cells, A549-ISG15$^{-/-}$ and the
564 A549-ISG15$^{-/-}$:prI5-AA and A549-ISG15$^{-/-}$:prI5-GG derivatives. Cells grown to 60-70%
565 confluency in T25 flasks were treated with 1000 IU/ml IFN-α for 24, 48 and 72 h or left
566 untreated for 72h. Whole cell lysate protein digestion was performed as described before
567 (47) for each time point. For lysis, cells were washed twice with PBS, and 250 ml lysis buffer
568 added (6 M Guanidine/50 mM HEPES pH 8.5). Cells were scraped in lysis buffer, vortexed
569 extensively and then sonicated. Cell debris was removed by centrifuging at 21,000 g for 10
570 min, twice. For the Dithiothreitol (DTT) was added to a final concentration of 5 mM and
571 samples were incubated for 20 min. Cysteines were alkylated with 14 mM iodoacetamide and
572 incubated 20 min at room temperature in the dark. Excess iodoacetamide was quenched with
573 DTT for 15 min. Samples were diluted with 200 mM HEPES pH 8.5 to 1.5 M Guanidine followed
574 by digestion at room temperature for 3 h with LysC protease at a 1:100 protease-to-protein
575 ratio. Samples were further diluted with 200 mM HEPES pH 8.5 to 0.5 M Guanidine. Trypsin
576 was then added at a 1:100 protease-to-protein ratio followed by overnight incubation at 37°C.
577 The reaction was quenched with 5% formic acid, then centrifuged at 21,000 g for 10 min to
578 remove undigested protein. Peptides were subjected to C18 solid-phase extraction (SPE, Sep-
579 Pak, Waters) and vacuum-centrifuged to near-dryness.
580 Samples were prepared for TMT labelling as previously described (47). Desalted
581 peptides were dissolved in 200 mM HEPES pH 8.5 and 25 mg of peptide labelled with TMT
582 reagent. TMT reagents (0.8 mg) were dissolved in 43 ml anhydrous aceto- nitrile and 3 ml
583 added to peptide at a final acetonitrile concentration of 30% (v/v). Following incubation at
584 room temperature for 1 h, the reaction was quenched with hydroxylamine to a final
585 concentration of 0.3% (v/v). Sample labelling was performed using 16-plex labelling reagent
586 (ThermoFisher Scientific™ CAT# A44520) and TMT-labelled samples were combined at a
587 1:1:1:1:1:1:1:1:1:1:1:1:1:1:1:1 ratio. Samples were vacuum-centrifuged to near dryness and
588 subjected to C18 SPE (Sep-Pak, Waters). An unfractionated single shot was analysed initially
589 to ensure similar peptide loading across each TMT channel, thus avoiding the need for

590 excessive electronic normalization. As all normalisation factors were >0.5 and <2, data for
591 each singleshot experiment was analysed with data for the corresponding fractions to
592 increase the overall number of peptides quantified.
593 TMT-labelled tryptic peptides were subjected to pH reversed-phase (HpRP)
594 fractionation using an Ultimate 3000 RSLC UHPLC system (Thermo Fisher Scientific) equipped
595 with a 2.1 mm internal diameter (ID) x 25 cm long, 1.7 mm particle Kinetix Evo C18 column
596 (Phenomenex). Mass spectrometry data was acquired using an Orbitrap Lumos and an
597 ultimate 3000 RSLC nano UHPLC equipped with a 300 mm ID x 5 mm Acclaim PepMap m-
598 Precolumn (Thermo Fisher Scientific) and a 75 mm ID x 50 cm 2.1 mm particle Acclaim
599 PepMap RSLC analytical column was used as described before (47).
600
601 **Data analysis of MS spectra**
602 For MS3-based TMT, as previously described (47), TMT tags on lysine residues and
603 peptide N termini (229.162932 Da) and carbamidomethylation of cysteine residues (57.02146
604 Da) were included as static modifications. Proteins were quantified by summing TMT reporter
605 ion counts across all matching peptide-spectral matches using 'MassPike', as described
606 previously (48). Briefly, a 0.003 Th window around the theoretical m/z of each reporter ion
607 (126, 127 n, 128 n) was scanned for ions, and the maximum intensity nearest to the the-
608 oretical m/z was used. An isolation specificity filter with a cutoff of 50% was employed to
609 minimise peptide co-isolation (48). Peptide-spectral matches with poor quality MS3 spectra
610 (more than 3 TMT channels missing and/or a combined S:N ratio of less than 100 across all
611 TMT reporter ions) or no MS3 spectra at all were excluded from quantitation. Peptides
612 meeting the stated criteria for reliable quantitation were then summed by parent protein, in
613 effect weighting the contributions of individual peptides to the total protein signal based on
614 their individual TMT reporter ion yields. Protein quantitation values were exported for further
615 analysis in Excel.
616 For protein quantitation, reverse and contaminant proteins were removed, then each
617 reporter ion channel was summed across all quantified proteins and normalised assuming
618 equal protein loading across all channels. Protein hits quantified by a single peptide were
619 removed from the dataset. The expression profile of each protein was observed after
620 comparing protein abundance to the condition (cell line/time point) with the highest MS

621 intensity score (set to 1) and normalised values were plotted against each time point for each
622 cell line (see Plotter in Supplementary File 1)
623
624 **Pathway Analysis**
625 To identify individual ISGs from our dataset, a list of 7112 gene symbols were searched
626 in 'Interferome v2.01' (http://interferome.its.monash.edu.au/interferome/home.jspx) (49).
627 The Interferome analysis was conducted on fold change values, which were calculated by
628 dividing the MS intensity score of each identified protein at a given time point post IFN
629 treatment (24, 48, 72 h) by the MS intensity score of the untreated control for each cell line.
630 A protein hit was considered to be an ISG if it was upregulated at least 1.7-fold in A549 control
631 cells following IFN-α treatment.
632 The Database for Annotation, Visualization and Integrated Discovery (DAVID) version
633 6.8 (https://david.ncifcrf.gov) was used to stringently identify cell line-specific enriched
634 pathways. An 'enrichment ratio' for each protein was obtained for each time point as follows
635 (MIS is MS intensity score):
636 $$Enrichment\ ratio = \left(\frac{Test\ cells\ MIS\ IFNa\ treated}{Test\ cells\ MIS\ untreated}\right) / \left(\frac{Control\ cells\ MIS\ IFNa\ treated}{Control\ cells\ MIS\ untreated}\right)$$
637 Protein hits upregulated at least 1.7-fold following enrichment were submitted using the
638 UniProt accession number and default medium classification stringency. Clusters were
639 considered significant if the Benjamini-Hochberg adjusted p-value was <0.05.
640 In the interest of simplicity, here we present the bioinformatic analyses only for the
641 48-h time point, which best represents the phenotypes observed in this experiment.
642
643 **Data availability**
644 The mass spectrometry proteomics data have been deposited to the
645 ProteomeXchange Consortium (http://www.proteomexchange.org) via the PRIDE (50)
646 partner repository with the dataset identifier (Accession # here).
647
648 **Figures**
649 Figures 1A, 2A, 6C and 9 were created with Biorender.com.

650

**Acknowledgments**

We are indebted to technical assistance provided by Dan Young. This work was supported by grants from the Academy of Medical Sciences (SBF003/1028 to DJH), Wellcome Trust Institutional Strategic Support Fund (to DJH), Wellcome Trust (101788/Z/13/Z to RER), the UK Medical Research Council (MC_UU_12014/1 to JM and CGGB) and by the Wellcome Trust via a Senior Clinical Research Fellowhship to MPW (108070/Z/15/Z).

659 **References**


660 1. Ivashkiv LB, Donlin LT. Regulation of type I interferon responses. Nat Rev Immunol.
661 2014;14(1):36–49.
662 2. Isaacs A, Lindenmann J. Virus Interference. I. The Interferon. Proc R Soc London Ser B
663 - Biol Sci. 1957;147(927):258–67.
664 3. Kim SH, Cohen B, Novick D, Rubinstein M. Mammalian type I interferon receptors
665 consists of two subunits: IFNaR1 and IFNaR2. Gene. 1997 Sep;196(1–2):279–86.
666 4. Gauzzi MC, Velazquez L, McKendry R, Mogensen KE, Fellous M, Pellegrini S.
667 Interferon-alpha-dependent activation of Tyk2 requires phosphorylation of positive
668 regulatory tyrosines by another kinase. J Biol Chem. 1996 Aug 23;271(34):20494–500.
669 5. Li X, Leung S, Kerr IM, Stark GR. Functional subdomains of STAT2 required for
670 preassociation with the alpha interferon receptor and for signaling. Mol Cell Biol.
671 1997 Apr;17(4):2048–56.
672 6. Potter JL, Narasimhan J, Mende-Mueller L, Haas AL. Precursor processing of pro-
673 ISG15/UCRP, an interferon-β-induced ubiquitin-like protein. J Biol Chem.
674 1999;274(35):25061–8.
675 7. Narasimhan J, Wang M, Fu Z, Klein JM, Haas AL, Kim JP. Crystal Structure of the
676 Interferon-induced Ubiquitin-like. 2005;280(29):27356–65.
677 8. Zou W, Papov V, Malakhova O, Kim K Il, Dao C, Li J, et al. ISG15 modification of
678 ubiquitin E2 Ubc13 disrupts its ability to form thioester bond with ubiquitin. Biochem
679 Biophys Res Commun. 2005 Oct 14;336(1):61–8.
680 9. Zhang D, Zhang D-E. Interferon-Stimulated Gene 15 and the Protein ISGylation
681 System. J Interf Cytokine Res. 2011;31(1):119–30.
682 10. Villarroya-beltri C, Guerra S, Sa F. ISGylation – a key to lock the cell gates for
683 preventing the spread of threats. 2017;2961–9.
684 11. Malakhov MP, Malakhova OA, Il Kim K, Ritchie KJ, Zhang DE. UBP43 (USP18)
685 specifically removes ISG15 from conjugated proteins. J Biol Chem.
686 2002;277(12):9976–81.
687 12. Ketscher L, Hannß R, Moralese DJ, Basters A, Guerra S, Goldmann T, et al. Selective
688 inactivation of USP18 isopeptidase activity in vivo enhances ISG15 conjugation and
689 viral resistance. Proc Natl Acad Sci U S A. 2015;112(5):1577–82.
690 13. Malakhova OA, Kim K Il, Luo J-K, Zou W, Suresh Kumar KG, Fuchs SY, et al. UBP43 is a

691 novel regulator of interferon signaling independent of its ISG15 isopeptidase activity.
692 EMBO J. 2006;25:2358–67.
693 14. Arimoto KI, Löchte S, Stoner SA, Burkart C, Zhang Y, Miyauchi S, et al. STAT2 is an
694 essential adaptor in USP18-mediated suppression of type i interferon signaling. Nat
695 Struct Mol Biol. 2017;24(3):279–89.
696 15. François-Newton V, de Freitas Almeida GM, Payelle-Brogard B, Monneron D, Pichard-
697 Garcia L, Piehler J, et al. USP18-based negative feedback control is induced by type I
698 and type III interferons and specifically inactivates interferon α response. PLoS One.
699 2011;6(7).
700 16. Wilmes S, Beutel O, Li Z, Francois-Newton V, Richter CP, Janning D, et al. Receptor
701 dimerization dynamics as a regulatory valve for plasticity of type I interferon
702 signaling. J Cell Biol. 2015;209(4):579–93.
703 17. Bogunovic D, Byun M, Durfee LA, Abhyankar A, Sanal O, Mansouri D, et al.
704 Mycobacterial Disease and Impaired IFN-γ Immunity in Humans with Inherited ISG15
705 Deficiency. Science (80- ). 2012;337:1684–9.
706 18. Zhang X, Bogunovic D, Payelle-Brogard B, Francois-Newton V, Speer SD, Yuan C, et al.
707 Human intracellular ISG15 prevents interferon-α/β over-amplification and auto-
708 inflammation. Nature. 2015;517(7532):89–93.
709 19. Martin-Fernandez M, Bravo García-Morato M, Gruber C, Murias Loza S, Malik MNH,
710 Alsohime F, et al. Systemic Type I IFN Inflammation in Human ISG15 Deficiency Leads
711 to Necrotizing Skin Lesions. Cell Rep. 2020;31(6):107633.
712 20. Speer SD, Li Z, Buta S, Payelle-Brogard B, Qian L, Vigant F, et al. ISG15 deficiency and
713 increased viral resistance in humans but not mice. Nat Commun. 2016;7(11496):DOI:
714 10.1038/ncomms11496.
715 21. Holthaus D, Vasou A, Bamford CGG, Andrejeva J, Paulus C, Randall RE, et al. Direct
716 Antiviral Activity of IFN-Stimulated Genes Is Responsible for Resistance to
717 Paramyxoviruses in ISG15-Deficient Cells. J Immunol. 2020;205(1):261–71.
718 22. Meuwissen MEC, Schot R, Buta S, Oudesluijs G, Tinschert S, Speer SD, et al. Human
719 USP18 deficiency underlies type 1 interferonopathy leading to severe pseudo-TORCH
720 syndrome. J Exp Med. 2016 Jun 27;213(7):1163–74.
721 23. Vuillier F, Li Z, Commere PH, Dynesen LT, Pellegrini S. USP18 and ISG15 coordinately
722 impact on SKP2 and cell cycle progression. Sci Rep. 2019;9(1):1–11.

723 24. Der SD, Zhou A, Williams BR, Silverman RH. Identification of genes differentially
724 regulated by interferon alpha, beta, or gamma using oligonucleotide arrays. Proc Natl
725 Acad Sci U S A. 1998 Dec 22;95(26):15623–8.
726 25. Liu SY, Sanchez DJ, Aliyari R, Lu S, Cheng G. Systematic identification of type I and
727 type II interferon-induced antiviral factors. Proc Natl Acad Sci U S A.
728 2012;109(11):4239–44.
729 26. Ivashkiv LB. IFNγ: signalling, epigenetics and roles in immunity, metabolism, disease
730 and cancer immunotherapy. Nat Rev Immunol. 2018;18(9):545–58.
731 27. Didcock L, Young DF, Goodbourn S, Randall RE. The V protein of simian virus 5 inhibits
732 interferon signalling by targeting STAT1 for proteasome-mediated degradation. J
733 Virol. 1999 Dec;73(12):9928–33.
734 28. Basters A, Geurink PP, Röcker A, Witting KF, Tadayon R, Hess S, et al. Structural basis
735 of the specificity of USP18 toward ISG15. Nat Publ Gr. 2017;24(3):270–8.
736 29. Basters A, Knobeloch KP, Fritz G. How USP18 deals with ISG15-modified proteins:
737 structural basis for the specificity of the protease. FEBS J. 2018;285(6):1024–9.
738 30. Arimoto K, Löchte S, Stoner SA, Burkart C, Zhang Y, Miyauchi S, et al. STAT2 is an
739 essential adaptor in USP18-mediated suppression of type I interferon signaling. Nat
740 Publ Gr. 2017;24(3):279–89.
741 31. Farrell PJ, Broeze RJ, Lengyel P. Accumulation of an mRNA and protein in interferon-
742 treated Ehrlich ascites tumour cells. Nature. 1979 Jun;279(5713):523–5.
743 32. Löchte S, Waichman S, Beutel O, You C, Piehler J. Live cell micropatterning reveals the
744 dynamics of signaling complexes at the plasma membrane. J Cell Biol.
745 2014;207(3):407–18.
746 33. Arimoto K-I, Miyauchi S, Stoner SA, Fan J-B, Zhang D-E. Negative regulation of type I
747 IFN signaling. J Leukoc Biol. 2018 Jun;103(6):1099–116.
748 34. Loeb KR, Haas AL. The interferon-inducible 15-kDa ubiquitin homolog conjugates to
749 intracellular proteins. J Biol Chem. 1992 Apr 15;267(11):7806–13.
750 35. Lenschow DJ, Giannakopoulos N V, Gunn LJ, Johnston C, O'Guin AK, Schmidt RE, et al.
751 Identification of interferon-stimulated gene 15 as an antiviral molecule during Sindbis
752 virus infection in vivo. J Virol. 2005 Nov 15;79(22):13974–83.
753 36. Catic A, Ploegh HL. Ubiquitin--conserved protein or selfish gene? Trends Biochem Sci.
754 2005 Nov 1;30(11):600–4.

755 37. Daczkowski CM, Dzimianski J V., Clasman JR, Goodwin O, Mesecar AD, Pegan SD.
756 Structural Insights into the Interaction of Coronavirus Papain-Like Proteases and
757 Interferon-Stimulated Gene Product 15 from Different Species. J Mol Biol.
758 2017;429(11):1661–83.
759 38. Dzimianski J V., Scholte FEM, Bergeron É, Pegan SD. ISG15: It's Complicated. J Mol
760 Biol. 2019 Oct 4;431(21):4203–16.
761 39. van den Elsen PJ. Expression regulation of major histocompatibility complex class I
762 and class II encoding genes. Front Immunol. 2011;2:48.
763 40. Rettino A, Clarke NM. Genome-wide Identification of IRF1 Binding Sites Reveals
764 Extensive Occupancy at Cell Death Associated Genes. J Carcinog Mutagen. 2013;(Spec
765 Iss Apoptosis).
766 41. Ma W, Lehner PJ, Cresswell P, Pober JS, Johnson DR. Interferon-γ rapidly increases
767 peptide transporter (TAP) subunit expression and peptide transport capacity in
768 endothelial cells. J Biol Chem. 1997;272(26):16585–90.
769 42. White LC, Wright KL, Felix NJ, Ruffner H, Reis LFL, Pine R, et al. Regulation of LMP2
770 and TAP1 genes by IRF-1 explains the paucity of CD8+ T cells in IRF-1(-/-) mice.
771 Immunity. 1996;5(4):365–76.
772 43. Chatterjee-Kishore M, LWright K, P-YTing J, RStark G. How Stat1 mediates constitutive
773 gene expression: a complex of unphosphorylated Stat1 and IRF1 supports
774 transcription of the LMP2 gene. EMBO J. 2000;19(15):4111–22.
775 44. Demaison C, Parsley K, Brouns G, Scherr M, Battmer K, Kinnon C, et al. High-Level
776 Transduction and Gene Expression in Hematopoietic Repopulating Cells Using a
777 Human Imunodeficiency Virus Type 1-Based Lentiviral Vector Containing an Internal
778 Spleen Focus Forming Virus Promoter. Hum Gene Ther. 2002 May 6;13(7):803–13.
779 45. He B, Paterson RG, Ward CD, Lamb RA. Recovery of infectious SV5 from cloned DNA
780 and expression of a foreign gene. Virology. 1997 Oct 27;237(2):249–60.
781 46. Randall RE, Young DF, Goswami KK, Russell WC. Isolation and characterization of
782 monoclonal antibodies to simian virus 5 and their use in revealing antigenic
783 differences between human, canine and simian isolates. J Gen Virol. 1987;68:2769–
784 80.
785 47. Nightingale K, Lin KM, Ravenhill BJ, Davies C, Nobre L, Fielding CA, et al. High-
786 Definition Analysis of Host Protein Stability during Human Cytomegalovirus Infection

787 Reveals Antiviral Factors and Viral Evasion Mechanisms. Cell Host Microbe.
788 2018;24(3):447-460.e11.
789 48. McAlister GC, Nusinow DP, Jedrychowski MP, Wühr M, Huttlin EL, Erickson BK, et al.
790 MultiNotch MS3 enables accurate, sensitive, and multiplexed detection of differential
791 expression across cancer cell line proteomes. Anal Chem. 2014;86(14):7150–8.
792 49. Rusinova I, Forster S, Yu S, Kannan A, Masse M, Cumming H, et al. INTERFEROME
793 v2.0: An updated database of annotated interferon-regulated genes. Nucleic Acids
794 Res. 2013;41(D1):1040–6.
795 50. Vizcaíno JA, Csordas A, Del-Toro N, Dianes JA, Griss J, Lavidas I, et al. 2016 update of
796 the PRIDE database and its related tools. Nucleic Acids Res. 2016;44(D1):D447–56.
797
798

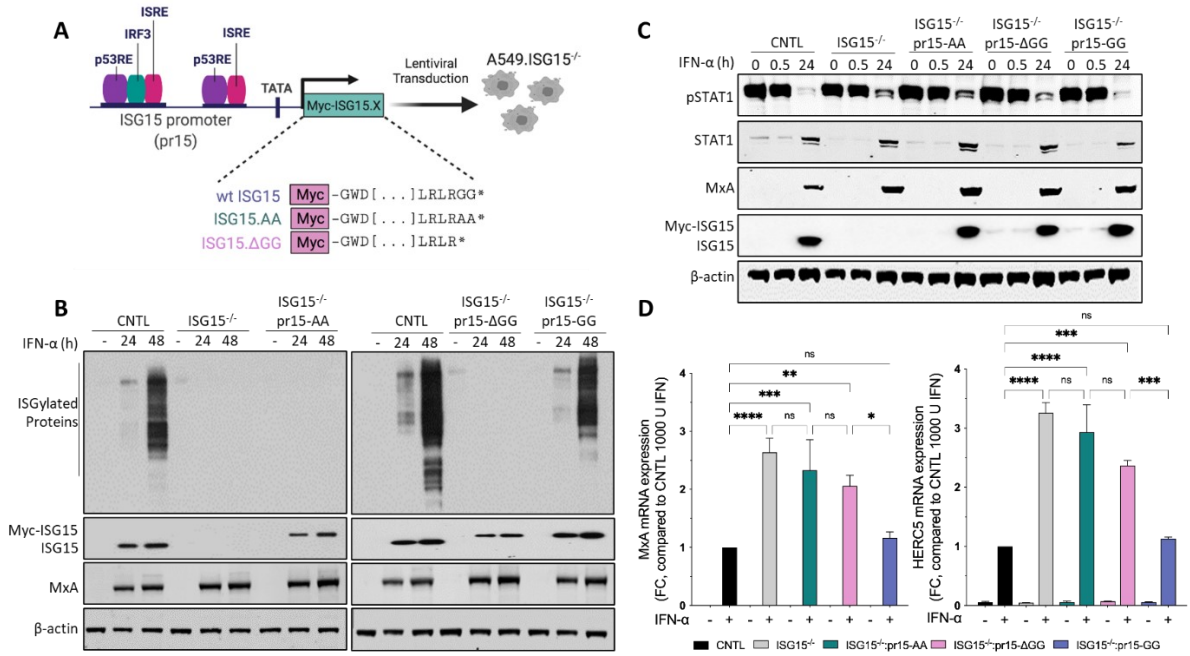


**Figure 1. Functional characterisation of A549-ISG15$^{-/-}$ cell lines reconstituted with the C-terminal ISG15 mutants, ISG15.AA and ISG15.ΔGG, or wild type ISG15, ISG15.GG. (A)** Schematic presentation of the lentiviral technology used to reconstitute ISG15 expression in A549-ISG15$^{-/-}$ using an inducible system where expression of ISG15 is under the control of its native promoter (pr15). The induction of pr15 is regulated by transcription factors physiologically upregulated by innate immune responses (e.g., IRF3 and ISGF3) or cell-cycle regulators (e.g. p53) **(B)** Immunoblot analysis of ISG15 expression induced by IFN-α treatment. A549 (CNTL), ISG15$^{-/-}$ and ISG15.AA-, ΔGG-, GG-expressing derivatives were treated with 1000 IU/ml IFN-α for 24 and 48 h or left untreated. Whole cell extracts were prepared and ISG15, MxA and β-actin proteins were analysed by immunoblot. **(C)** A549 (CNTL), 1SG15$^{-/-}$ and ISG15.AA-, ΔGG-, GG-expressing derivatives were treated with 1000 IU/ml IFN-α for 30 min, then extensively washed and media without IFN replaced. Cells were harvested at 0 and 30 min and 24 h after IFN-α removal and phopho-STAT1, total STAT1, MxA, ISG15 and β-actin were detected by immunoblot. Data in lanes 1 – 6 have previously been reported (21) **(D)** A549 (CNTL), ISG15$^{-/-}$ and ISG15.AA-, ΔGG-, GG-expressing derivatives were treated with 1000 IU/ml IFN-α for 24 h. Expression of ISGs was tested using reverse transcription quantitative PCR (RT-qPCR) with primers specific for *MxA* and *HERC5*. Relative expression was determined following SYBR Green quantitative PCR (qPCR) using ΔΔCt method. *β-Actin* expression was used to normalize between samples. Data are presented as a mean fold increase relative to IFN-α-treated A549 control cells (set to 1). Error bars represent the SD of the mean from three independent experiments performed on different occasions. Each experiment additionally included three technical replicates. Statistical significance was assessed using two-way ANOVA and Tukey multiple comparisons test; *, $p < 0.05$, **, $p < 0.01$, ***, $p < 0.001$, ****, $p < 0.0001$, n.s., no statistical significance.

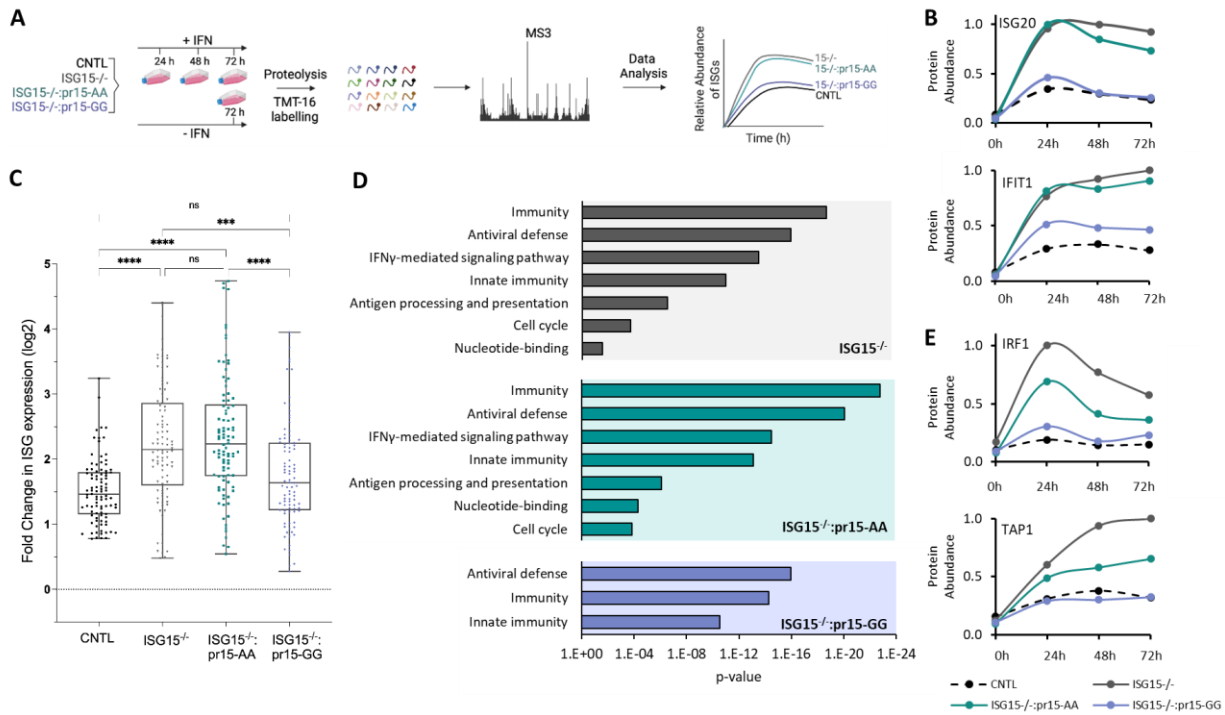


**Figure 2. Quantitative temporal analysis of proteomes from IFN-α-treated ISG15$^{-/-}$ and reconstituted cells (A)** Schematic presentation of the experimental workflow. **(B)** Abundance of representative examples of well-known ISGs over time after IFN-α simulation, normalised to a maximum of 1 for each protein. **(C)** Comparative quantitative analysis of ISG expression in A549 (CNTL), A549-ISG15$^{-/-}$ and ISG15.AA- or ISG15.GG-expressing cells. ISGs were defined by (a) correspondence with the Interferome database and (b) >1.7-fold increase in abundance in IFN-a stimulated compared to unstimulated A549 control cells. Statistical significance was assessed using one-way ANOVA and Tukey multiple comparisons test; ***, $p < 0.001$, ****, $p < 0.0001$, n.s., no statistical significance**. (D)** Pathway analysis using DAVID software. Proteins >1.7-fold upregulated following IFN-α treatment in each cell type compared to A549 control cells were searched using DAVID software using the default medium classification stringency. Benjamini-Hochberg adjusted p-values are shown. **(E)** Expression profiles of representative examples of well-characterised factors with roles in IFN-γ signalling and antigen processing and presentation pathways. Protein abundance was calculated as described in (B).

838

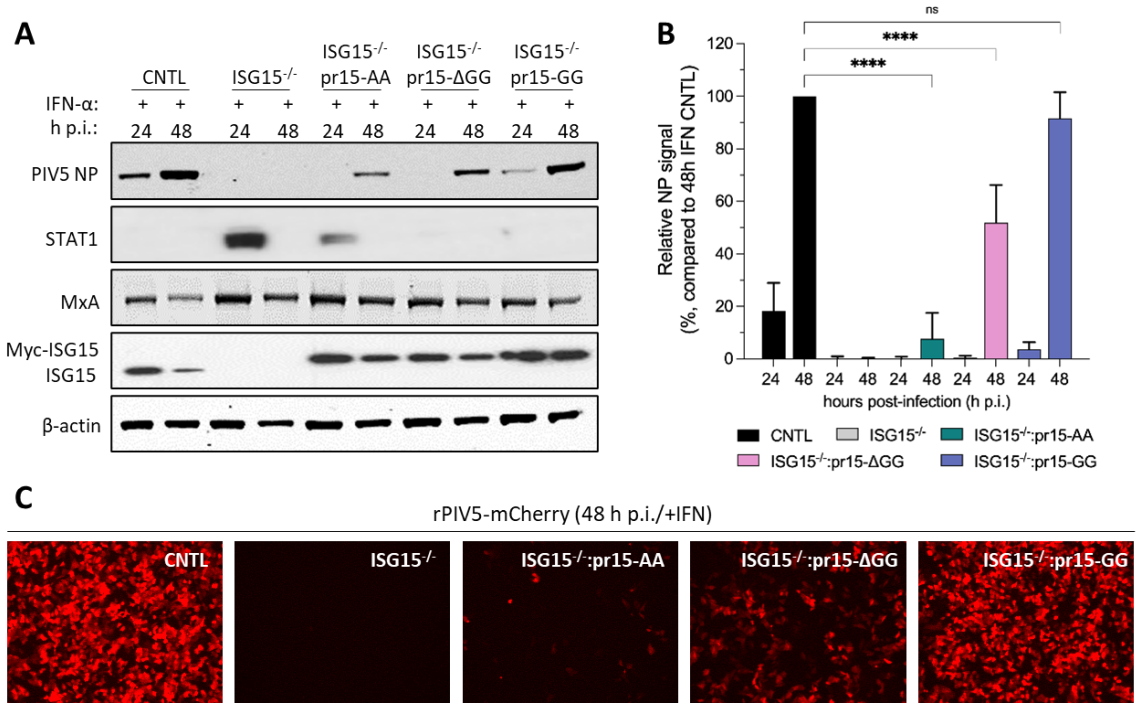


839

840

841 **Figure 3. The ability of ISG15 C-terminus to regulate IFN-α signalling influences viral infection (A)**
842 A549 (CNTL), ISG15$^{-/-}$ and ISG15.AA-, ISG15.ΔGG- and ISG15.GG-expressing derivatives were treated
843 with 1000 IU/ml IFN-α for 18 h and then infected with rPIV5-cherry (MOI 10). Cells were harvested at
844 24 and 48 h p.i. and processed for immunoblot analysis using antibodies specific for PIV5 NP, STAT1,
845 MxA, ISG15 and β-actin. **(B)** Experiments described in (A) were performed independently three times
846 (infections were performed on three separate occasions), and NP and β-actin levels were quantified
847 using Image Studio software (LI-COR Biosciences). Signals were relative to those generated from IFN-
848 α-treated A549 cells infected for 48 h p.i. (set to 100%). Error bars = SD. Statistical significance was
849 assessed using two-way ANOVA and Tukey multiple comparisons test; ****, $p < 0.0001$, n.s., no
850 statistical significance. **(C)** Fluorescent imagining of mCherry expression, indicative of rPIV5-mCherry
851 infection, at the 48 hours post infection (h.p.i.) time point described in (A).

852

853

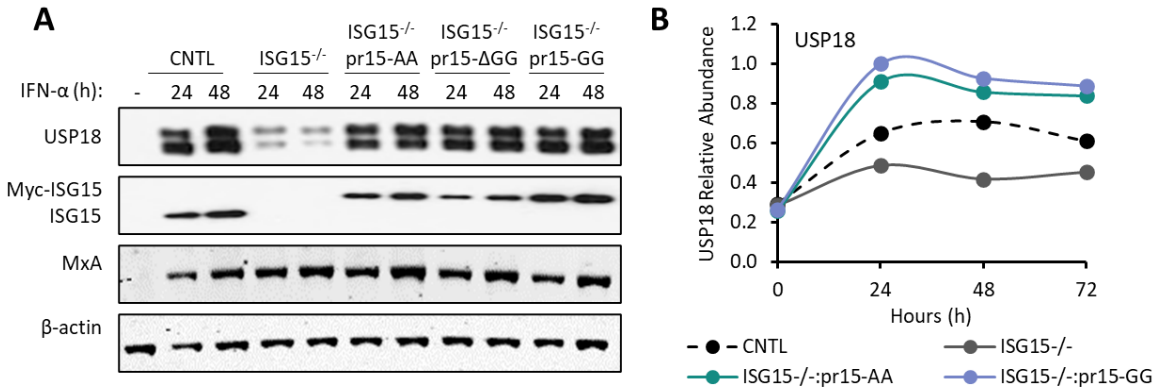


854

855

856 **Figure 4. The C-terminal di-Gly motif of ISG15 is not required for USP18 stabilisation**. **(A)** Immunoblot
857 analysis of USP18 expression in A549 (CNTL), ISG15$^{-/-}$ and ISG15.AA-, ΔGG-, GG-expressing derivatives
858 after treatment with 1000 IU/ml IFN-α for 24 h. Whole cell extracts were prepared and USP18, ISG15,
859 MxA and β-actin protein levels were analysed by immunoblot. **(B)** USP18 abundance in A549 (CNTL),
860 ISG15$^{-/-}$ and ISG15.AA and ISG15.GG-expressing derivative cells measured using quantitative tandem
861 mass tags (TMT)-based proteomic analysis (see Figure 2).

862

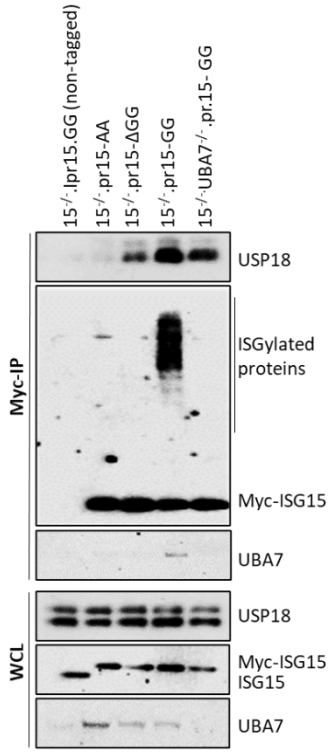


**Figure 5. The C-terminal di-Gly motif of ISG15 is crucial for the ISG15-USP18 interaction.** Immunoprecipitation of Myc-tagged ISG15 expressed in ISG15.AA-, ΔGG-, GG-expressing cell lines after treatment with 1000 IU/ml IFN-α for 24 h. An ISG15$^{-/-}$ cell-line expressing a non-tagged form of ISG15 was used as a negative control (left lane) and an ISG15.GG-expressing 1SG15$^{-/-}$.UBA7$^{-/-}$ cell line was used as an ISGylation-deficient control (final lane). ISG15 was immunoprecipitated (IP) using anti-c-Myc antibodies covalently coupled to magnetic beads. Immunoprecipitates (top) and whole cell lysates (WCL; bottom) were subject to immunoblot analysis with antibodies to USP18, ISG15 and UBA7. ISG15 expression in reconstituted cell lines was under the control of the ISG15 promoter (pr15) and was therefore inducible by IFN.

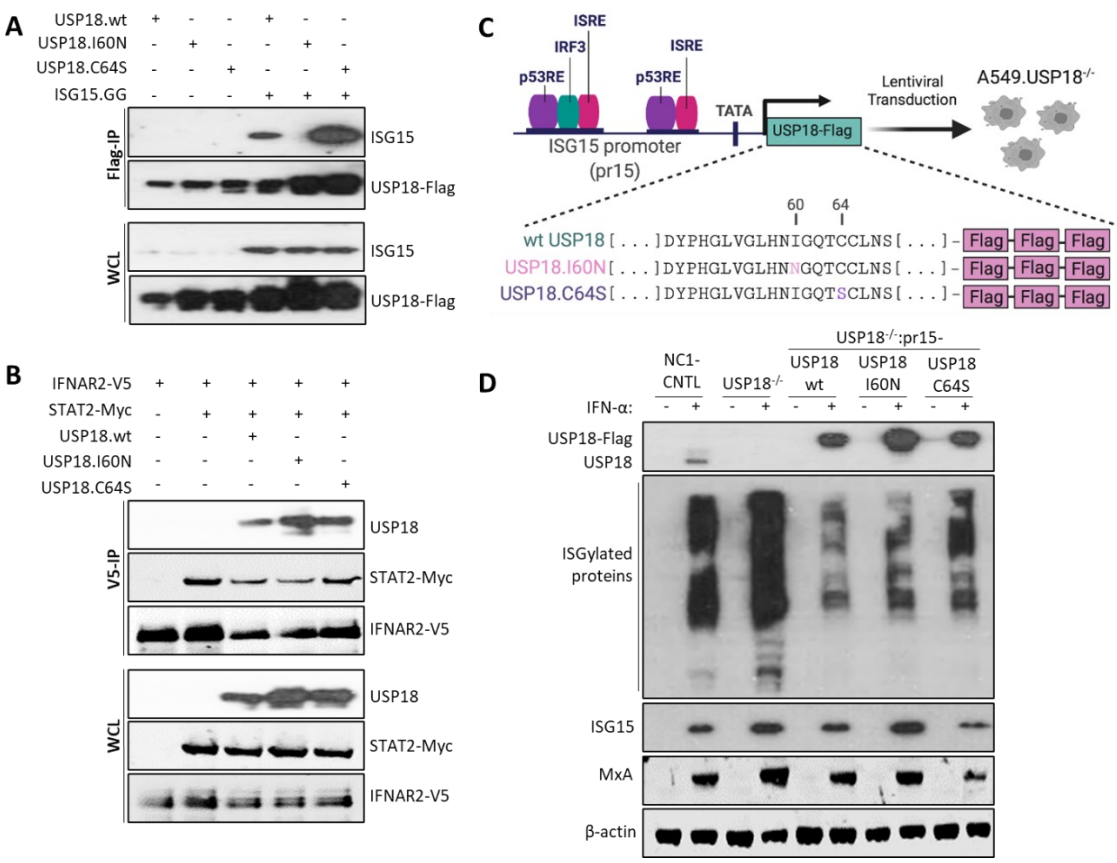


**Figure 6. Functional characterisation of catalytically inactive and ISG15-binding mutants of USP18** **(A)** Immunoprecipitation of Flag-tagged wt and mutant forms of USP18 in HEK293T cells co-transfected with wt ISG15 (ISG15.GG) as indicated. Cells were lysed 48 h post-transfection and lysates were immunoprecipitated with Flag-specific antibodies covalently coupled to magnetic beads. Immunoprecipitates (top) and whole cell lysates (WCL; bottom) were subject to immunoblot with antibodies to USP18 and ISG15. **(B)** Immunoprecipitation of V5-tagged IFNAR2 cytoplasmic domain in HEK293T cells co-transfected with STAT2-Myc, USP18.wt-Flag, USP18.I60N-Flag or USP18.C64S-Flag plasmids as indicated. Cells were lysed at 48 h post-transfection and lysates were immunoprecipitated with anti-V5 antibody coupled to protein G dynabeads. Immunoprecipitates (V5-IP; top) and whole cell lysates (WCL; bottom) were subject to immunoblot with antibodies to anti-V5 epitope tag, STAT2and USP18. **(C)** Schematic presentation of the lentiviral technology used to reconstitute USP18 expression in A549-USP18$^{-/-}$ using an inducible system where USP18 expression is driven by the ISG15 promoter (pr15). **(D)** Immunoblot analysis of USP18 expression induced by IFN-α treatment. A549 (CNTL), USP18$^{-/-}$ and USP18.wt-,I60N-,C64S-expressing cell lines were treated with 1000 IU/ml IFN-α for 48 h or left untreated. Whole cell extracts were prepared and USP18, ISG15, MxA and β-actin protein levels were analysed by immunoblot.

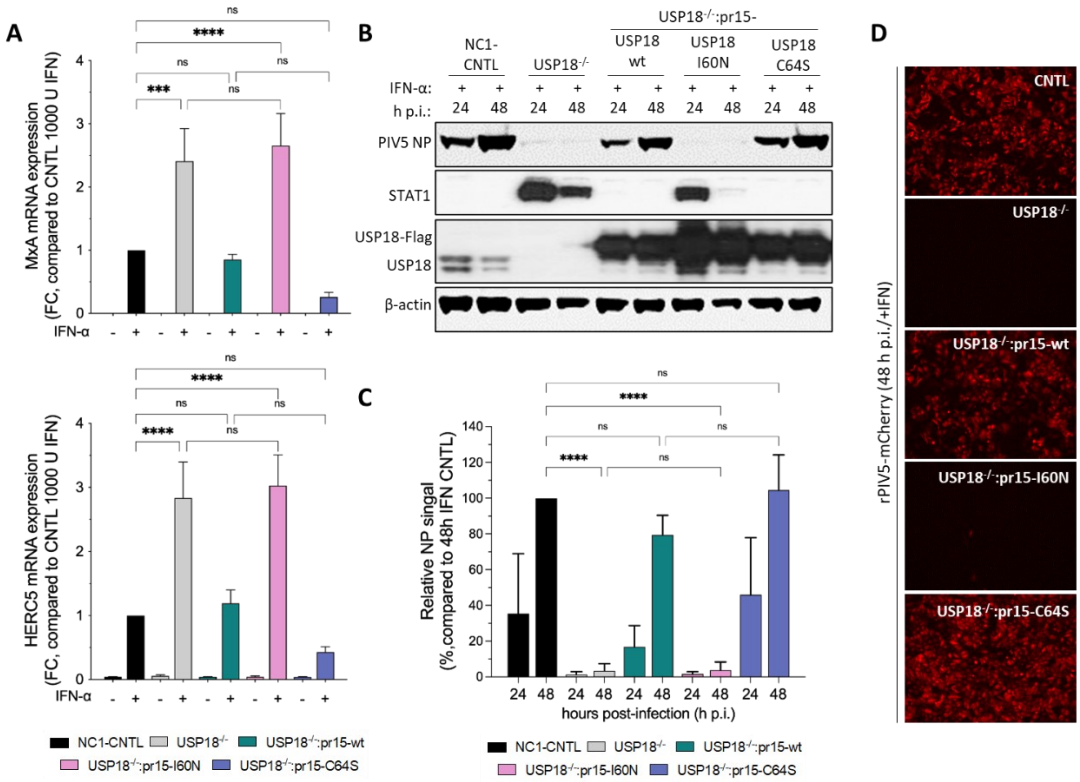


**Figure 7. ISG expression is dysregulated in cells expressing USP18 mutant unable to bind ISG15. (A)** A549 control cells expressing NC1 non targeting guide RNA (NC1-CNTL), A549-USP18$^{-/-}$ and USP18.wt, I60N-, C64S-expressing derivatives (where USP18 expression was under the control of the ISG15 promoter (pr15) and therefore inducible by IFN) were treated with 1000 IU/ml IFN-α for 16 h. Expression of ISGs was tested using reverse transcription quantitative PCR (RT-qPCR) with primers specific for *MxA* and *HERC5*. Relative expression was determined following SYBR Green quantitative PCR (qPCR) using ΔΔCt method. *β-Actin* expression was used to normalize between samples. Data shown represent mean values from three independent experiments performed on different occasions; error bars = SD. Statistical significance was assessed using two-way ANOVA and Tukey multiple comparisons test; *, $p < 0.05$, **, $p < 0.01$, ***, $p < 0.001$, n.s., no statistical significance. **(B)** A549 NC1-CNTL, A549-USP18$^{-/-}$ and USP18.wt-, I60N-, C64S-expressing derivatives were pre-treated with 1000 IU/ml IFN-α for 16 h and then infected with rPIV5-mCherry (MOI 10). Cells were harvested at 24 and 48 h.p.i. and processed for immunoblot analysis using antibodies specific for PIV5 NP, STAT1, USP18 and β-actin. **(C)** Experiments described in (B) were performed independently three times (infections were performed on three separate occasions), and NP and β-actin levels were quantified using Image Studio software (LI-COR Biosciences). Signals were normalised to IFN-α-treated A549 cells infected for 48 h p.i. (set to 100%). Data shown represent mean values from three independent experiments; error bars = SD. Statistical significance was assessed using two-way ANOVA and Tukey multiple comparisons test; ****, $p < 0.0001$, n.s., no statistical significance. **(D)** Fluorescent imagining

933 of mCherry expression, indicative of rPIV5-mCherry infection, at 48h p.i time point of experiment
934 described in (B).

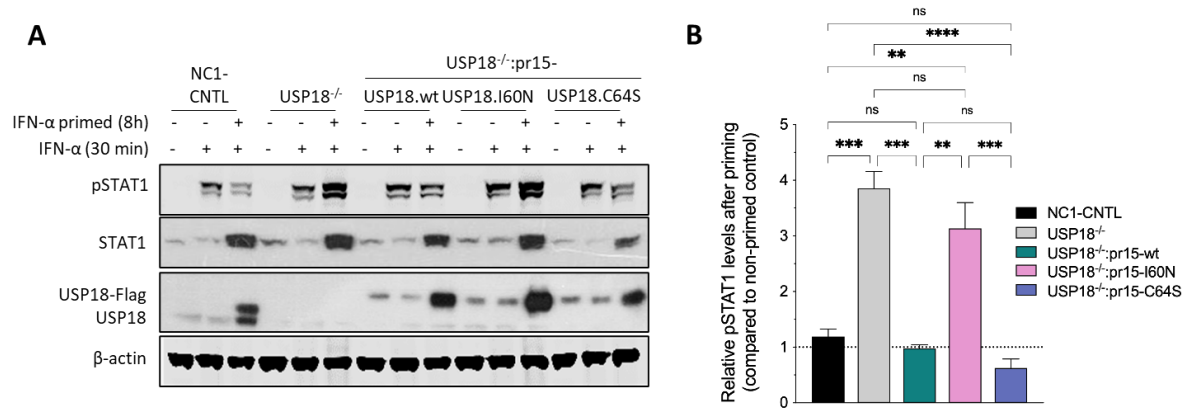


935
936
937
938 **Figure 8. The ISG15-USP18 interaction is important for desensitization of IFN-α signalling. (A)** A549
939 control cells expressing NC1 non targeting guide RNA (NC1-CNTL), A549-USP18$^{-/-}$ and USP18.wt-, I60N,
940 C64S-expressing cells were primed with 2000 IU/ml IFN-α (equivalent to 20 ng/ml) for 8 h or left
941 untreated. Cells were washed, and re-incubated in medium without IFN for 16 h and then stimulated
942 with 2000 IU/ml IFN-α for 30 min. Cell lysates were subject to immunoblot analysis with antibodies to
943 anti-phospho-STAT1, USP18 and β-actin. **(B)** Experiments described in (A) were performed
944 independently three times, and phospho-STAT1 and β-actin levels were quantified using Image Studio
945 software (LI-COR Biosciences). Signals are presented as ratios of primed to non-primed control (a ratio
946 of 1 is equivalent to no change). Data shown represent mean values from three independent
947 experiments; error bars = SD. Statistical significance was assessed using one-way ANOVA and Tukey
948 multiple comparisons test; *, $p < 0.05$, **, $p < 0.01$, ***, $p < 0.001$, ****, $p < 0.0001$, n.s., no statistical
949 significance.
950

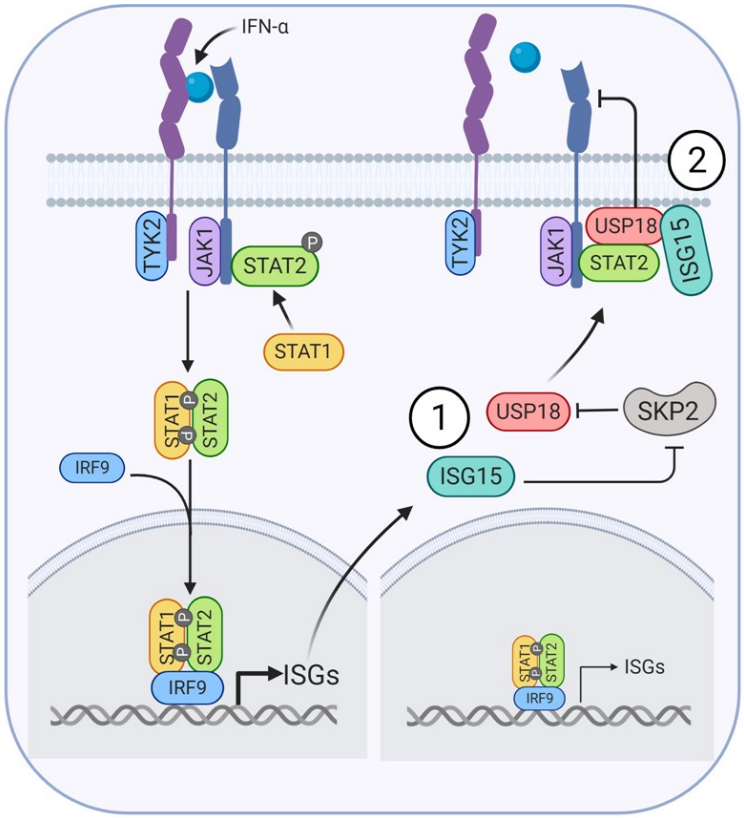


**Figure 9. Model.** IFN-α, expressed as a consequence of infection, binds to IFNAR and induces the formation of the IFNAR1-IFNAR2-IFN-α ternary complex. Signalling is transduced through the JAK/STAT pathway, culminating in the expression of several hundreds of ISGs. As ISGs, both USP18 and ISG15 are expressed and are both known to regulate the magnitude of type I IFN signalling. ISG15 promotes USP18 stability (1) by preventing SKP2-mediated ubiquitination and proteasomal degradation of USP18, making it available for STAT2-dependent recruitment to IFNAR2 and to inhibit ternary complex formation. How ISG15 protects USP18 from degradation is not known, but this does not require an interaction between ISG5 and USP18. Separately, through non-covalent interactions dependent on its C-terminal di-Gly, ISG15 facilitates USP18's inhibitory function (2). It is not currently known whether this interaction occurs at the receptor, or prior to USP18's recruitment to IFNAR2.